THE BELL SYSTEM
TECHNICAL JOURNAL

DEVOTED TO THE SCIENTIFIC AND ENGINEERING
ASPECTS OF ELECTRICAL COMMUNICATION

Volume 54 November 1975 Number 9

Excitation of Parabolic-Index Fibers With Incoherent Sources

By D. MARCUSE

(Manuscript received May 5, 1975)

We study the excitation of a parabolic-index fiber by an incoherent source. The theory is based on approximating the fiber modes by Laguerre-gaussian functions. The dependence of the total light power injected into the fiber core on the separation between source and fiber, and on the transverse displacement of the source, is shown in graphic form. Also shown are far-field radiation patterns, which indicate the distribution of power versus mode number, for several launching conditions and plots of power versus azimuthal mode number for given values of the compound mode number. The study of launching efficiency versus source radius leads to prescriptions for optimizing the ratio of source to fiber core radius without a matching lens. Use of a lens for matching the image of a small source to the size of the fiber core increases the launching efficiency relative to the power consumption of the light-emitting-source diode.

I. INTRODUCTION

The excitation of step-index fibers (fibers whose cores have a constant index of refraction surrounded by a lower index cladding) has been investigated by several authors by means of ray optics.[1,2] In this paper, we study the excitation of fibers with a core whose refractive indices have a square-law dependence on the radial dimension (parabolic-index fibers). The fibers are assumed to support many modes and are excited by an incoherent source—for example, a light-emitting diode (LED). Our analysis is based on wave optics. We assume that we

may use the Laguerre-gaussian modes of the infinite square-law medium to approximate the modes of the parabolic-index fiber. Lower-order modes do not carry significant amounts of power in the region of the core boundary so that they are approximated very well by the Laguerre-gaussian modes of the infinite medium. We introduce the effect of the core boundary by considering the Laguerre-gaussian modes as being cut off when their propagation constants become equal to the plane wave propagation constant of the cladding material.

The Laguerre-gaussian modes have the advantage that they not only approximate the modes of the parabolic-index fiber, but they are also approximate solutions of beam waves in free space. The free-space modes have a beam width parameter that is a function of the z coordinate (distance from the fiber measured in the direction of its axis). At the fiber end, the free-space Laguerre-gaussian modes match the fiber modes. Thus, it is only necessary to calculate the excitation of the free-space Laguerre-gaussian beam modes by the incoherent source, if we assume that the space surrounding the fiber is matched to the fiber core (at least approximately) by means of an index-matching fluid.

We study the excitation of the modes of the parabolic-index fiber as functions of the source radius, its distance from the fiber, and as a function of its transverse displacement. This study provides information about the tolerance requirements for aligning the source with respect to the fiber. We also discuss the optimization of the source diameter with regard to the total power delivered to the fiber and with regard to the excitation efficiency relative to the electrical power required to drive the source.

We conclude that the tolerance requirements for placing the source are modest and that either the total amount of power or the power excitation efficiency of the fiber can be optimized by a suitable choice of the source diameter. It is assumed that the fiber, as well as the source, have circular cross sections.

Equation (29) states a simple law for the total amount of light power that may be injected into a parabolic-index fiber by an incoherent source of brightness B [Δ is defined by eq. (18)]. The normalization used for the power plotted in Figs. 4 through 10 is based on the expression for the total number of guided modes (28).

The efficiency of the system could be improved considerably by use of a lens or taper to match the light output of a small-area incoherent source to the core of the fiber. Use of lenses or tapers may be undesirable because such matching devices introduce added complexity into the system. However, if high overall efficiency is an important requirement, matching of the output of a small-area LED to the fiber

core with the help of an additional optical system offers a means of increasing the launching efficiency.

II. EXCITATION OF MODES BY AN INCOHERENT SOURCE

We consider a complete orthogonal set of modes obeying the orthonormality condition[3,4]

$$\frac{1}{2}\int_A (\mathbf{E}_\nu \times \mathbf{H}_\mu^*)\cdot \mathbf{e}_z dxdy = P\delta_{\nu\mu}. \tag{1}$$

The symbols $\mathbf{E}_\nu$ and $\mathbf{H}_\mu$ indicate the electric and magnetic field vectors of the modes labeled ν or μ, $\mathbf{e}_z$ is a unit vector in z direction, A is the infinite cross-sectional area of the structure, and $\delta_{\nu\mu}$ is the Kronecker delta symbol. The factor P is a normalizing constant with the dimension of power. It is assumed to be the same for all the modes.

The total electric field can be expressed as the superposition of all the modes,[4]

$$\mathbf{E} = \sum_{\nu=1}^{\infty} c_\nu \mathbf{E}_\nu. \tag{2}$$

The total power carried by the field may be expressed as[4]

$$P_t = \sum_{\nu=1}^{\infty} P\langle |c_\nu|^2\rangle. \tag{3}$$

It can be shown that a current with current density $\mathbf{j}$ excites each mode according to the formula,[5]

$$c_\nu = -\frac{1}{4P}\int_V \mathbf{j}\cdot\mathbf{E}_\nu^* dV. \tag{4}$$

The integral is extended over the volume in which the current density $\mathbf{j}$ exists; P is the normalizing parameter encountered in (1) and (3).

We are now ready to apply this formalism to the excitation of modes by an incoherent source. As a model of an incoherent source, we consider a disc of circular cross section with radius b and thickness t. The current density inside of the disc is assumed to be a random function with vanishing correlation length. The ensemble average of the absolute square magnitude of (4) is

$$\langle |c_\nu|^2\rangle = \frac{1}{16P^2}\int_V dV \int_V dV' \mathbf{E}_\nu^*\cdot\langle \mathbf{jj}^*\rangle\cdot\mathbf{E}_\nu'. \tag{5}$$

The quantity $\langle \mathbf{jj}^*\rangle$ appearing in (5) is a tensor of second rank. However, we consider that the current in the source is composed of many randomly oriented and randomly phased dipoles. This assumption allows us to assume that the off-diagonal elements of the tensor

vanish, and that all diagonal elements are equal. Thus, the tensor reduces to a multiple of the unit tensor I, and we may write

$$\langle \mathbf{jj}^* \rangle = SI\delta(\mathbf{r} - \mathbf{r}'). \tag{6}$$

Using (6) reduces (5) to the simpler form

$$\langle |c_\nu|^2 \rangle = \frac{tS}{16P^2} \int_{A_s} \mathbf{E}_\nu^* \cdot \mathbf{E}, dxdy. \tag{7}$$

A_s is the area of the circular cross section of the source disc.

If we apply the formula (7) to the plane-wave modes of free space, we can calculate the amount of power ΔP that is flowing through the element of solid angle $d\Omega$ in a given direction in space. This calculation results in the expression

$$\Delta P = \frac{\omega\mu_0 St}{16\pi^2} A_s n k d\Omega, \tag{8}$$

where

$$k = \omega\sqrt{\epsilon_0\mu_0}$$

$$n = \text{refractive index of the medium.}$$

The derivation of (8) is sketched in the appendix.

Our model of an incoherent source behaves like a Lambert-law radiator except for a missing factor $\cos\theta$, where θ is the angle between the direction of observation and the normal direction to the surface of the disc. The factor $\cos\theta$ is missing in our theory because we treated the source as being transparent to radiation. In a partially opaque source, radiation leaving the source must originate in a volume with an effective thickness t as seen in the direction of observation. It is shown in Fig. 1 that the effective thickness of the source disc depends

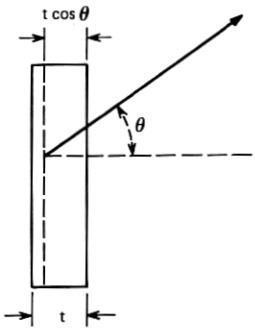

Fig. 1—Schematic of a partially opaque source disc. The effective width for waves emitted at a normal angle to the surface is t; for waves emitted at an angle θ, the effective width is $t \cos\theta$.

on the direction of observation so that we must replace t with $t \cos \theta$. Modified for the case of a partially opaque source, eq. (8) assumes the form

$$\Delta P = BA_s \cos \theta d\Omega. \tag{9}$$

The brightness of the source is defined as

$$B = \frac{\omega \mu_0 Stnk}{16\pi^2}. \tag{10}$$

Equation (10) relates the product St to the measurable quantity B. If we introduce the z component β of the propagation constant nk by the equation

$$\beta = nk \cos \theta \tag{11}$$

and modify (7) for the case of a partially opaque source, we may write

$$P\langle |c_\nu|^2 \rangle = \frac{\pi^2 B}{\omega \mu_0 nkP} \frac{\beta}{nk} \int_{A_s} \mathbf{E}_\nu^* \cdot \mathbf{E}_\nu dxdy. \tag{12}$$

The left-hand side of this expression indicates the power carried by the mode labeled ν. This power is provided by the incoherent source with brightness B. The brightness is the amount of power that the unit area of the source radiates into the unit solid angle, its dimension is W/cm^2 sr (sr = steradians).

Equation (12) is the starting point for our discussion of the excitation of the modes of the parabolic-index fiber by an incoherent source.

III. EXCITATION OF LAGUERRE-GAUSSIAN MODES

The Laguerre-gaussian beam modes of free space, normalized to carry the power P, may be expressed as follows:[6,7]

$$\mathbf{E}_{\nu,p} = \left\{ \frac{2^{\nu+3}}{e_\nu \pi w_0^2 n} \sqrt{\frac{\mu_0}{\epsilon_0}} \frac{p!}{(p+\nu)!} P \right\}^{\frac{1}{2}} \cdot \frac{w_0}{w} \left(\frac{r}{w} \right)^\nu e^{-(r/w)^2} L_p^{(\nu)} \left(\frac{2r^2}{w^2} \right) \cos \nu\phi e^{i\psi}, \tag{13}$$

with

$$e_\nu = \begin{cases} 2 & \text{for } \nu = 0 \\ 1 & \text{for } \nu \neq 0 \end{cases}. \tag{14}$$

The beamwidth parameter is defined by the formula ($k = \omega(\epsilon_0 \mu_0)^{\frac{1}{2}}$, n is the refractive index of "free space")

$$w = w_0 \left[1 + \left(\frac{2z}{nkw_0^2} \right)^2 \right]^{\frac{1}{2}}, \tag{15}$$

and the phase function is given as

$$\psi = -nkz + (\nu + 2p + 1) \arctan\left(\frac{2z}{nkw_0^2}\right) - \frac{nkr^2}{2R}, \tag{16}$$

with the phase front radius of curvature

$$R = z\left[1 + \left(\frac{nkw_0^2}{2z}\right)^2\right]. \tag{17}$$

$\mathbf{E}_{\nu,p}$ is the x or y component of the electric field vector of the Laguerre-gaussian beam mode. Thus, the electric field is linearly polarized but is expressed in a cylindrical coordinate system with the coordinates r, ϕ, and z. We may replace the function cos $\nu\phi$ by sin $\nu\phi$ without changing any other parameter in (13). Thus, the modes are degenerate in the sense that two orthogonal polarizations, as well as both choices of the ϕ symmetry (sin $\nu\phi$ or cos $\nu\phi$), are allowed for each set of mode numbers ν, p. The function $L_p^{(\nu)}$ is a Laguerre polynomial.[8]

The origin of the z coordinate is at the narrowest point of the field distribution where we have $w = w_0$. The minimum beam width w_0 is arbitrary. However, the Laguerre-gaussian beam modes are equal to the modes of the square-law medium,[9] with refractive index distribution

$$n = n_0\left[1 - \left(\frac{r}{a}\right)^2 \Delta\right], \tag{18}$$

if we set $w = w_0$ and use[3]

$$w_0 = \left[\frac{a}{n_0 k}\sqrt{\frac{2}{\Delta}}\right]^{\frac{1}{2}}. \tag{19}$$

This choice of the beamwidth parameter w_0 ensures that, at $z = 0$, the transverse field distribution of the Laguerre-gaussian mode of free space coincides with the mode of the square-law medium (18). Both types of modes, the beam modes of free space and the modes of the square-law medium, are only approximate solutions that apply in the paraxial approximation that holds for small values of the refractive index parameter Δ and, for free space modes, for modes with sufficiently large values of w_0. For values of z other than $z = 0$, the phase function of the modes of the square-law medium must be expressed as

$$\psi = -\beta z \tag{20}$$

with the propagation constant

$$\beta = \left[n_0^2 k^2 - \frac{2n_0 k}{a}\sqrt{2\Delta}(2p + \nu + 1)\right]^{\frac{1}{2}}. \tag{21}$$

If we assume that free space consists of a medium whose refractive index n is matched to an average value of the fiber core, reflection from

the fiber end is negligibly small. We assume that the fiber core has radius a and that its refractive index is given by (18) in the region $0 \leqq r \leqq a$. In the cladding at $r > a$, the refractive index assumes the constant value

$$n_2 = n_0(1 - \Delta). \tag{22}$$

The mode fields (13) [with $w = w_0$ of (19)] approximate the modes of the parabolic-index fiber at radius $r < a$ for small values of ν and p. For large values of the mode numbers ν and p, the fields extend strongly beyond $r = a$ so that (13) (with $w = w_0$) is no longer a good approximation to the fiber modes. However, modes reaching strongly into the cladding are no longer guided by the fiber core. For this reason, we regard (13) (with $w = w_0$) as an approximation for all guided fiber modes and consider the relation

$$\beta = n_2 k = n_0(1 - \Delta)k \tag{23}$$

as a cutoff condition for the guided modes.

Because the modes of the parabolic-index fiber join smoothly with the Laguerre-gaussian beam modes of free space, we obtain the excitation of the fiber modes by determining the excitation coefficients for the Laguerre-gaussian beam modes with the help of (12). Substitution of (13) into (12) results in

$$P\langle|c_{\nu,p}|^2\rangle = \frac{8\pi B}{e_\nu w^2 (nk)^2} \frac{p!2^\nu}{(p+\nu)!} \times \int_{A_s} \left(\frac{r}{w}\right)^{2\nu} e^{-2(r/w)^2} \left[L_p^{(\nu)}\left(\frac{2r^2}{w^2}\right)\right]^2 r dr d\phi. \tag{24}$$

The ratio β/k was approximated by unity. We have added the coefficients for the modes with $\cos \nu\phi$ to those of the $\sin \nu\phi$ symmetry and used the fact that the sum of the squares of cosine and sine is unity. The integration in (24) extends over the surface of the source A_s.

If the surface of the source is larger than the area over which the mode field exists with an appreciable amplitude, the integral can be performed with the result

$$P\langle|c_{\nu,p}|^2\rangle = \frac{4\pi^2 B}{e_\nu (nk)^2}. \tag{25}$$

For $\nu = 0$, there is only one type of mode because $\sin \nu\phi = 0$. For all other values of ν, we have lumped two modes together. If we express again only the power of a single mode of a given polarization and azimuthal symmetry, we have, instead of (25),

$$P\langle|c_{\nu,p}|^2\rangle = 2\left(\frac{\pi}{nk}\right)^2 B = \frac{1}{2}\left(\frac{\lambda_0}{n}\right)^2 B. \tag{26}$$

This is an interesting formula. First of all, it shows that each mode (of

the fiber or of the free-space beam modes) receives an equal amount of power if the incoherent source is large enough. Second, comparison of eq. (26) with (9) shows that each mode acts as though it receives radiation from a square of the source surface whose sides are equal to the wavelength and as if it collects all power radiated into the solid angle $\frac{1}{2}$ *sr*. It is now easy to determine the power that is collected by all the guided modes of the fiber. We need only multiply (26) by the number of modes. The total number of guided modes is obtained from (21) and the cutoff condition (23). Combining these two equations, we obtain the following equation for the boundary in mode number space:

$$(2p + \nu + 1)_{\max} = nka\sqrt{\frac{\Delta}{2}} = \left(\frac{a}{w_0}\right)^2. \tag{27}$$

Figure 2 shows the mode number space defined by the two variables ν and p. The diagonal line (the hypotenuse of the triangle) is defined by (27). The guided modes lie inside the triangle shown in the figure. The total number of modes is approximately equal to four times the area of this triangle. The factor 4 stems from the fact that for each set of values of ν and p, we have modes with two different polarizations and two different azimuthal symmetries (except for $\nu = 0$). Thus, the total number of modes is

$$N = (nka)^2 \frac{\Delta}{2}. \tag{28}$$

The total amount of power P_f injected by a large, incoherent source into a square-law fiber is given as the product of (26) and (28),

$$P_f = \pi(\pi a^2)B\Delta. \tag{29}$$

Equation (24) can be used to calculate the power in each mode for arbitrary position of the source in relation to the fiber. In general, we assume that the fiber is separated from the source by a distance z and that it is offset by an amount d as shown in Fig. 3. The Φ integration in

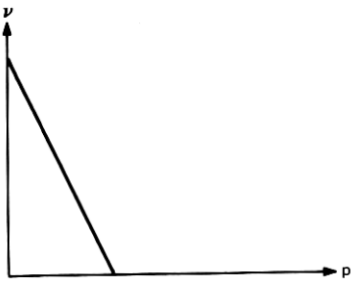

Fig. 2—Mode number plane p, ν. The diagonal line is the boundary of the guided modes that are contained inside the triangular region.

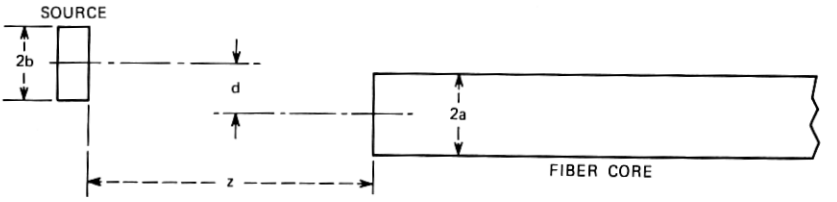

Fig. 3—Geometry of the source exciting a fiber core.

(24) can still be performed with the result

$$P\langle|c_{\nu,p}|^2\rangle = \frac{4\pi B}{(nk)^2 w^2}\frac{p!}{(p+\nu)!} \times \left\{2\pi \int_0^{|b-d|} \left(\frac{2r^2}{w^2}\right)^{\nu} e^{-2(r/w)^2}\left[L_p^{(\nu)}\left(\frac{2r^2}{w^2}\right)\right]^2 r\,dr + \int_{|b-d|}^{|b+d|} (\pi - 2\Phi_1)\left(\frac{2r^2}{w^2}\right)^{\nu} e^{-2(r/w)^2}\left[L_p^{(\nu)}\left(\frac{2r^2}{w^2}\right)\right]^2 r\,dr\right\}, \quad (30)$$

with

$$\Phi_1 = \arcsin\left(\frac{r^2 + d^2 - b^2}{2rd}\right). \quad (31)$$

Equation (30) applies again for one mode of given polarization and azimuthal symmetry. The integral in (30) must be evaluated numerically. The z dependence of the expression is hidden in the beamwidth parameter w according to (15).

IV. NUMERICAL EVALUATION AND RESULTS

In this section we show the results of numerical evaluations of eq. (30). We begin by discussing the dependence of the total power injected into the fiber on the distance between the source and the fiber end. All length variables are normalized with respect to the fiber radius a. Figure 4 shows the dependence of the normalized total power on z/a for a source whose radius is equal to the fiber radius, $b/a = 1$, for three values of Δ. The normalization of the power is apparent by comparison with (26). Since P_f indicates the total power carried by all the modes, we have divided it by the total number of modes N that is obtained from (28). This normalization results in unit normalized power at $z = 0$.

Figure 4 shows that, for $\Delta = 0.01$, the amount of power that is injected into the fiber by the incoherent source drops to approximately one-half of its maximum value for $z/a = 11$. Thus, the injection process is surprisingly insensitive to the separations between the source and the fiber end. We have checked that the curves of Fig. 4 do not change

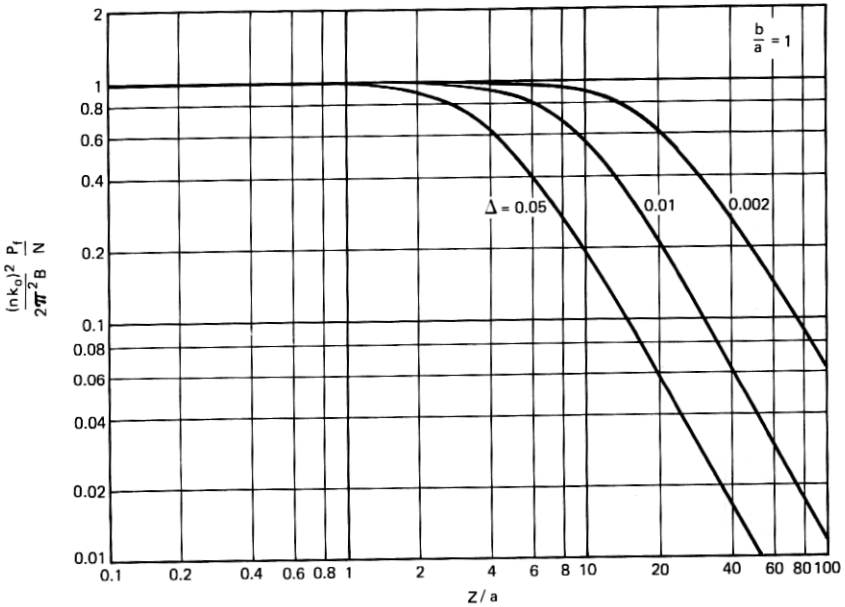

Fig. 4—Normalized total power P_f injected into the parabolic-index fiber as a function of the distance z between source and fiber. N is the total number of modes [see (28)]; B is the source brightness. This figure holds for a source-to-fiber core radius ratio $b/a = 1$.

if the value of ka is varied. Thus, the curves are universal, at least for large values of ka, that is, for fibers supporting a large number of modes. This dependence on k suggests that the curves may be derived by the methods of ray optics. The lowest part of the curves has almost reached an inverse square-law dependence on fiber-source separation. We have checked that a precise inverse square-law dependence is obtained for source-to-fiber ratios of $b/a = 0.1$. Thus, the inverse square law is reached rather slowly and will be realized by the curves of Fig. 4 for even larger values of z/a than those appearing in the figure. The curve with $\Delta = 0.01$ shows that a separation of the source from the fiber end equal to the fiber diameter, $z = 2a$, causes a drop in power coupling efficiency by only approximately 5 percent. The tolerance to source-fiber separation eases for smaller values of Δ. The curves do not reach exactly the value unity at $z = 0$ because the source is not infinitely wide. However, the slight departure from unity (0.3 percent for $N = 400$, $\Delta = 0.01$) is not apparent on the scale of the figure.

Figure 5 shows the dependence of the excitation efficiency on the amount of relative offset d/a for a source whose radius equals the fiber radius, $b/a = 1$, and which is located at three different distances from

the fiber end. The curves were computed for $\Delta = 0.01$. However, the shapes of the curves are universal and only their vertical positions depend on the value of Δ. It is immediately apparent from this figure that the relative tolerance to source displacements (offsets) becomes more liberal as the distance between the source and the fiber end is increased. A source displacement of $d/a = 1$ causes a drop in power to 40 percent of its maximum value if the source is placed directly at the fiber end, $z/a = 0$. For $z/a = 10$, the excitation efficiency has dropped from 0.55 to 0.34, that is, only 62 percent of its maximum value, for a transverse source displacement of $d/a = 1$. Like Fig. 4, Fig. 5 is independent of ka if this value is large.

So far we have concentrated on the total power injected into the fiber. It is interesting to consider the distribution of power over the various guided modes as the distance between the source and the fiber is increased. The far-field pattern emerging from the far end of the fiber (which is not facing the source) gives an indication of the mode distribution. Figure 6 shows the power density of the far-field radiation pattern as a function of angle α. The curves of this figure represent far-field radiation patterns for several values of the relative fiber-source distance z/a for $\Delta = 0.01$. The curves were obtained by taking the

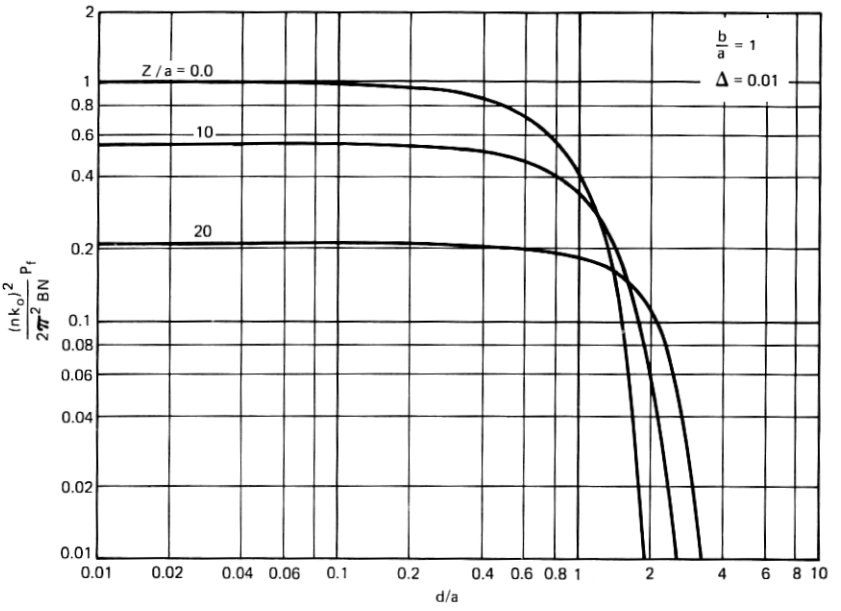

Fig. 5—Normalized total power injected into parabolic-index fiber as a function of the transverse source displacement d for several values of the distance z of the source from the fiber and for $\Delta = 0.01$.

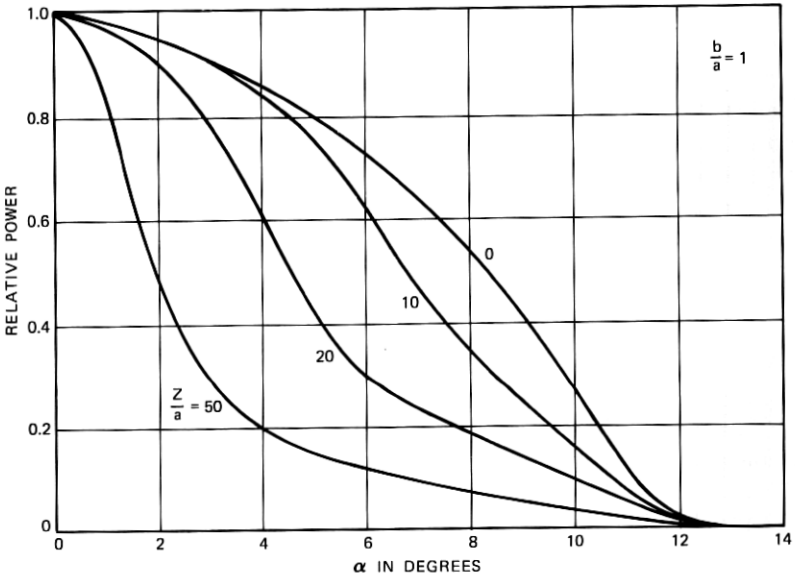

Fig. 6—Far-field radiation pattern. α is the angle (in degrees) of the direction of the observation point with respect to the fiber axis. The curves are arbitrarily normalized to unity at $\alpha = 0$. The source-to-fiber core radius ratio is $b/a = 1$, $\Delta = 0.01$.

ensemble average of the absolute square value of (2),

$$\langle |E|^2 \rangle = \sum_{\nu=1}^{N} \langle |c_\nu|^2 \rangle |\mathbf{E}_\nu|^2, \tag{32}$$

with the mode fields of (13) and the expansion coefficients of (30). All curves in Fig. 6 were computed for a source whose radius is equal to the fiber radius, $b/a = 1$, with no transverse source displacement, $d/a = 0$. The far-field pattern of a parabolic-index fiber with all modes equally excited corresponds to the curve labeled $z/a = 0$. As the source is moved away from the fiber end, the far-field radiation pattern narrows. This narrowing is caused by the fact that higher-order modes receive less power as the distance z is increased. The curves of Fig. 6 are normalized so that the power density at zero angles becomes unity.

Figures 7 through 9 give more detailed insight into the distribution of power versus mode number. Equation (21) shows that modes with equal values of the compound mode number,

$$M = 2p + \nu + 1, \tag{33}$$

have equal propagation constants. These modes lie on straight lines parallel to the diagonal line in mode-number space shown in Fig. 2. Figure 7 indicates the power distribution among the modes with

$M = 19$ that lie near the guided-mode boundary in mode-number space. If the source is placed directly in contact with the fiber, $z/a = 0$, all modes with $M = 19$ are almost equally excited, receiving almost the maximum of power. However, for $z/a = 4$, at a point where the total amount of power has dropped by only 8 percent from its maximum value, the highest-order mode group with $M = 19$ suffers a very substantial decrease in power. It is interesting that modes with higher values of ν receive more power (for constant values of M). This trend is reversed only for $z/a \geqq 8$.

Figure 8 shows the relative power in other mode groups at a fixed value of $z/a = 8$. Modes with low compound mode number, $M \leqq 6$, are still fully excited, but with increasing values of M the amount of power in the higher-order modes drops off. Figure 9 shows the same trend even more strongly for a source-fiber separation of $z/a = 20$.

So far we have studied the dependence of the excitation efficiency of the parabolic-index fiber on the source-fiber separation z/a and on the amount of offset d/a for $b/a = 1$. Figure 10 shows the normalized total amount of power for $z/a = 0$ as a function of the relative source radius b/a. This curve does not depend on the values of Δ or ka. As expected, the total amount of injected power drops off as b/a decreases. However, the decrease in total power is not proportional to the area of the source, as one might have expected, but is nearly proportional to

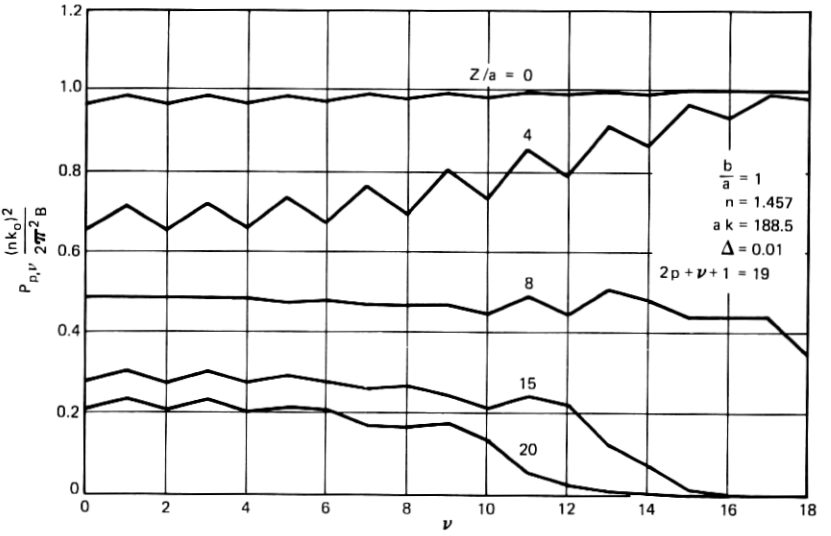

Fig. 7—Normalized power in a given mode belonging to the mode group with compound mode number $2p + \nu + 1 = 19$ as a function of the azimuthal mode number ν for several values of the distance z between source and fiber. These curves apply to the case $b/a = 1$, $ka = 188.5$, $\Delta = 0.01$, $n = 1.457$.

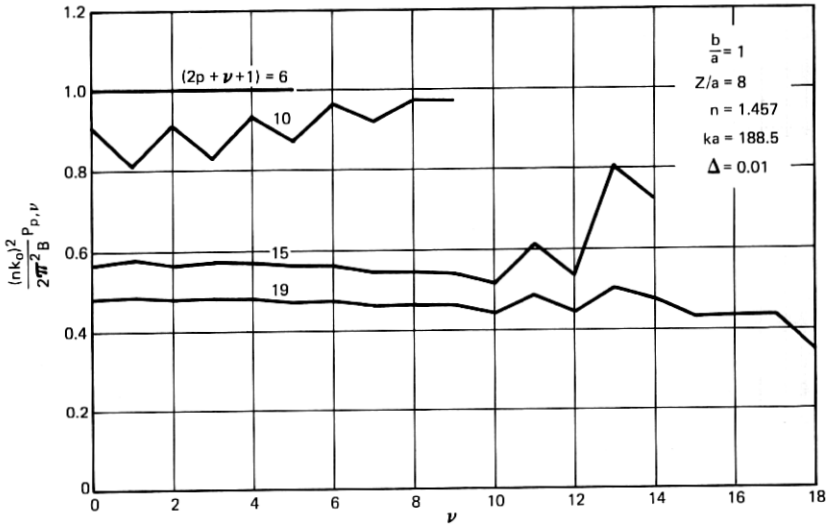

Fig. 8—Normalized power of individual modes belonging to the compound mode number $2p + \nu + 1$ (whose values are given in the figure) as a function of the azimuthal mode number ν. The source-to-fiber distance is $z/a = 8$, all other parameters are the same as in Fig. 7.

the source radius. This behavior has interesting consequences for the optimum choice of the source radius as is discussed in the next section.

Figure 11 shows far-field radiation patterns for several values of b/a. Comparison with Fig. 6 shows that the dependence of the far-field

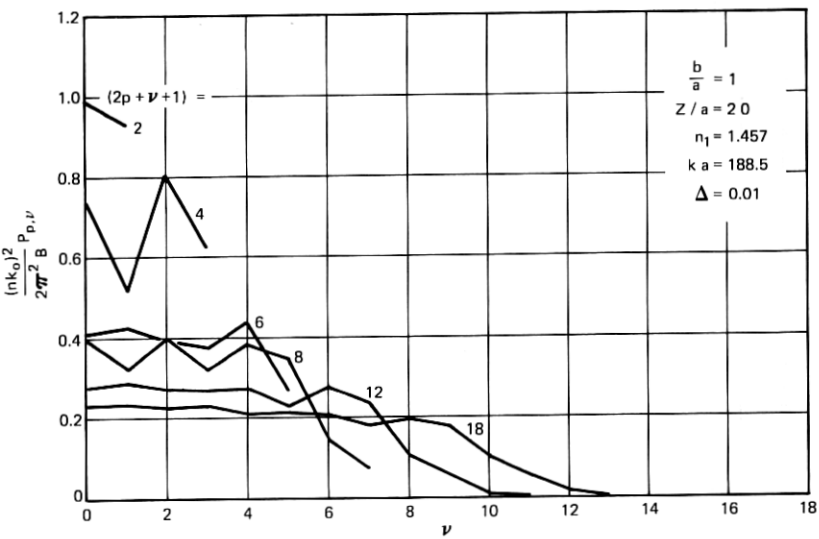

Fig. 9—This figure is similar to Fig. 8 with $z/a = 20$.

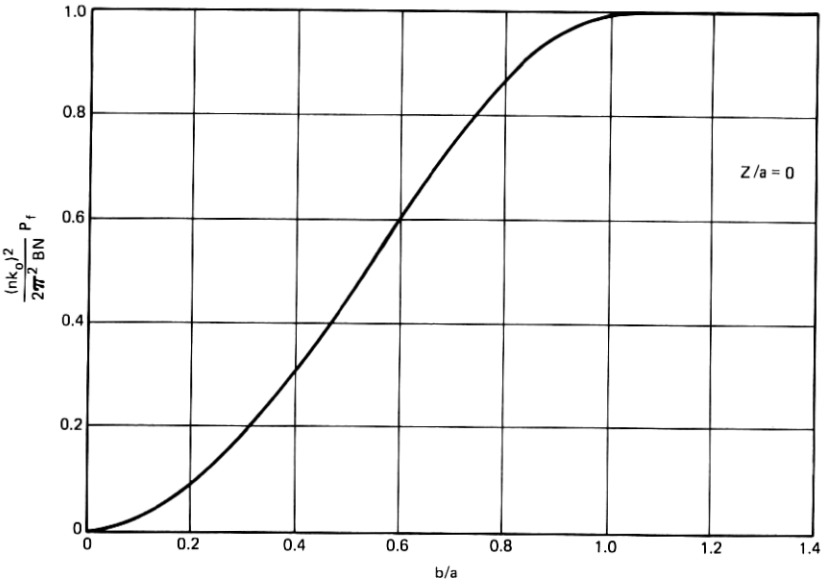

Fig. 10—Normalized total power as a function of the normalized source radius b. This figure is independent of ka and Δ.

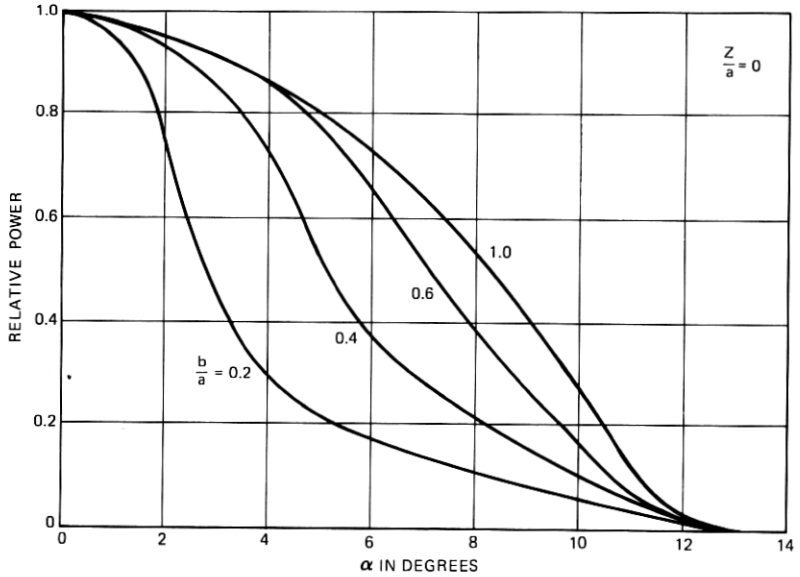

Fig. 11—Far-field radiation pattern from the end of the fiber for several values of the source-to-fiber core radius ratio b/a.

radiation patterns on the source radius bears a close resemblance to its dependence on the source-fiber separation. Higher-order modes are excited less strongly as the source radius decreases.

V. SOURCE OPTIMIZATION WITHOUT LENSES

If the source brightness B is held constant, more power is injected into the fiber as b/a increases to a value near unity. Beyond that value, no further advantage is to be gained. In fact, even though the total amount of injected power remains constant for $b/a > 1$, the overall efficiency decreases since regions of the source at $b > a$ do not contribute to the excitation of the fiber, but do waste their power. If brightness were independent of the dimensions of the source, the optimum source radius would be $b = a$. However, light-emitting diodes (LEDs) tend to be brighter if their radius decreases. C. A. Burrus has made measurements on a special type of LED operated at two-thirds of its saturation current that indicate that source brightness increases with decreasing radius.[10] This dependence is shown in Fig. 12, which was drawn from data given in Burrus' paper. The solid line is drawn

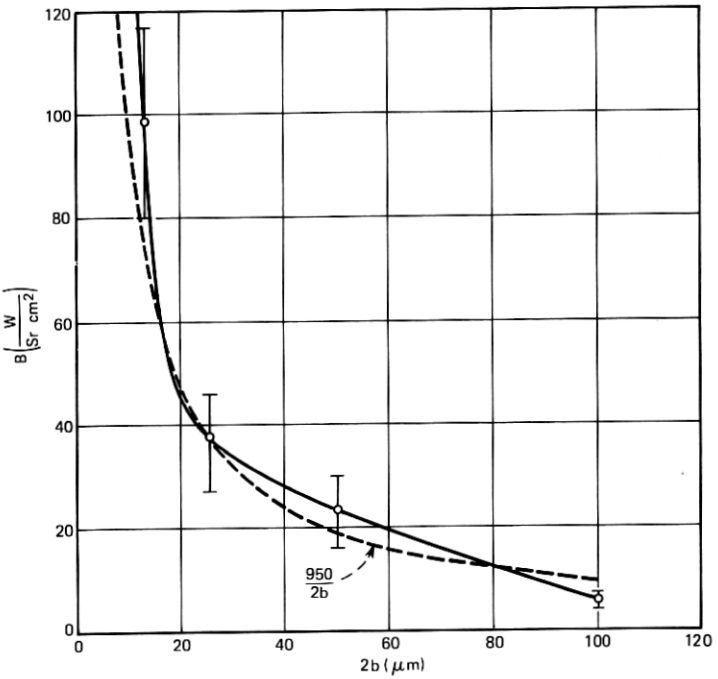

Fig. 12—Source brightness of high-intensity LEDs according to Ref. 10. The dotted line is an inverse $2b$ law used to approximate the solid curve.

through the average values, and the vertical error bars indicate the experimental uncertainty of the brightness measurements. The dotted line shown in Fig. 12 is the hyperbola

$$B = \frac{950}{2b} = \frac{W}{(b/a)} \tag{34}$$

that seems to approximate the experimental data reasonably well. To a rough approximation, the brightness of LEDs (at least of the Burrus type) seems to be inversely proportional to their radius.

To study the excitation efficiency as a function of source radius, we approximate the curve of Fig. 10 by the polynomial

$$\frac{(nk)^2}{2\pi^2}\frac{P_f}{N} = B\left[A_1\frac{b}{a} + A_2\left(\frac{b}{a}\right)^2 + A_3\left(\frac{b}{a}\right)^3\right] \tag{35}$$

with

$$\left.\begin{aligned} A_1 &= -0.06875 \\ A_2 &= 2.85 \\ A_3 &= -1.78125 \end{aligned}\right\}. \tag{36}$$

This third-order polynomial approximates the curve in Fig. 10 to within 1 percent. Substitution of (34) into (35) results in

$$\frac{(nk)^2}{2\pi^2}\frac{P_f}{WN} = A_1 + A_2\frac{b}{a} + A_3\left(\frac{b}{a}\right)^2. \tag{37}$$

This function is plotted in Fig. 13. Under the conditions prevailing in Burrus-type diodes, where the maximum attainable brightness depends on the source radius, the total power that can be injected by an LED in direct contact with a parabolic-index fiber has a maximum at a source radius of $b = 0.8a$. However, even for source radii as small as

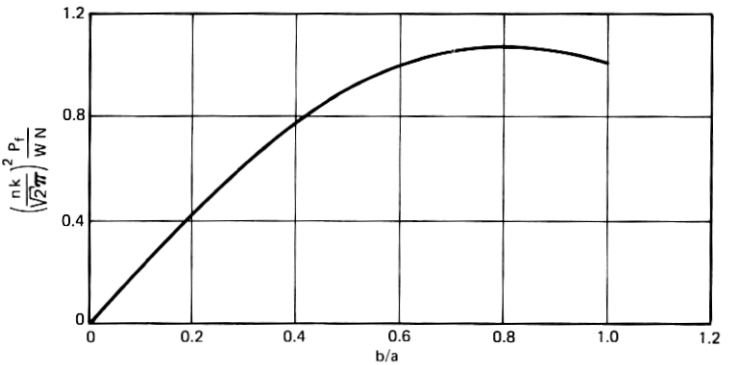

Fig. 13—Total power injected into the fiber with the high-brightness LEDs of Fig. 12 as a function of the (normalized) source radius b.

$b = 0.6a$, the total power in the fiber equals the amount that is obtained with an LED whose radius equals the fiber radius. This means that an LED with a radius only approximately half as large as that of the fiber core is still almost as effective as an LED whose radius equals the fiber core radius.

Disregarding the electrical input power into the LED, we would optimize the overall performance of the fiber system, operated without a matching lens, by choosing a source-to-fiber radius ratio of $b/a = 0.8$. However, a different optimum is obtained if we try to optimize the ratio of total power injected into the fiber to the power required to drive the diode. The power input to the LED can be estimated from the information contained in Burrus' paper[10] by multiplying the diode current with the energy gap voltage, V = 1.38 V at room temperature. This power estimate comes close to the actual power since the voltage developed across the LED's terminals varies between 1.35 and 1.6 V. Four points obtained for the LED's power consumption operated at two-thirds the saturation current are shown in Fig. 14 as a function of the diameter $2b$ of the diode. In the region between $2b = 0$ and $2b = 50$ μm, the power curve is approximately linear. According to the limited information that is available, the curve seems to turn over for larger values of $2b$. However, since only one point (at $2b = 100$ μm) does not lie on the straight line, the shape of the curve beyond $2b = 50$ μm is not known. For sufficiently small source radii, we approximate the curve in Fig. 14 by the equation

$$P_e = (8.5)(10^{-3})(2b) = W_e b/a, \tag{38}$$

keeping in mind that this linear law becomes questionable for $2b > 50$ μm. Substitution of (38) into (37) yields

$$\frac{(nk)^2}{2\pi^2}\frac{W_e}{NW}\frac{P_f}{P_e} = \frac{A_1}{b/a} + A_2 + A_3\frac{b}{a}. \tag{39}$$

This function is shown in Fig. 15. The maximum of the fiber excitation efficiency relative to the electrical drive power of the diode appears at $b/a = 0.2$, that is, at rather small source radii. It is important to remember that, even though Fig. 15 is drawn as a function of b/a, only b is allowed to vary while a must be kept constant because W_e, appearing in the normalization coefficient, is a function of a.

A good compromise between the maximum achievable total power and the desire to obtain good excitation efficiency relative to the power input to the LED may be to operate with a diode whose radius is approximately one-half of the fiber radius. In this case, $b/a = 0.5$, we lose 17 percent of the optimum operating power efficiency and work 19 percent below the maximum achievable injected power. But neither loss of efficiency is very serious and both requirements, low diode power

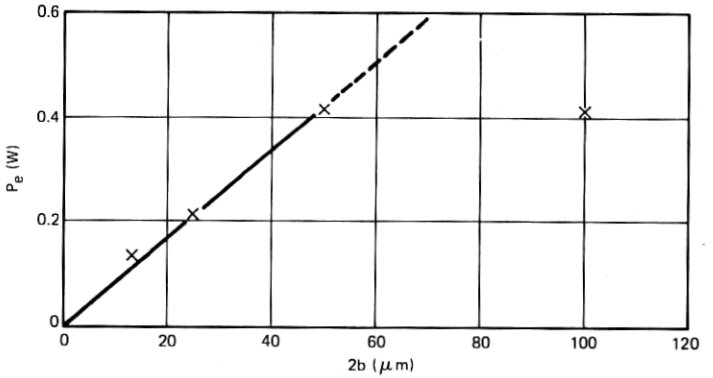

Fig. 14—Power consumption of the high-brightness LEDs as a function of source radius.

consumption and a large amount of total power launched into the fiber, are still approximately satisfied.

VI. OPERATION WITH A MATCHING LENS

Figure 10 shows that the amount of power launched into the parabolic-index fiber decreases with decreasing fiber core radius if the source brightness is held constant. The reason for this decrease in in-

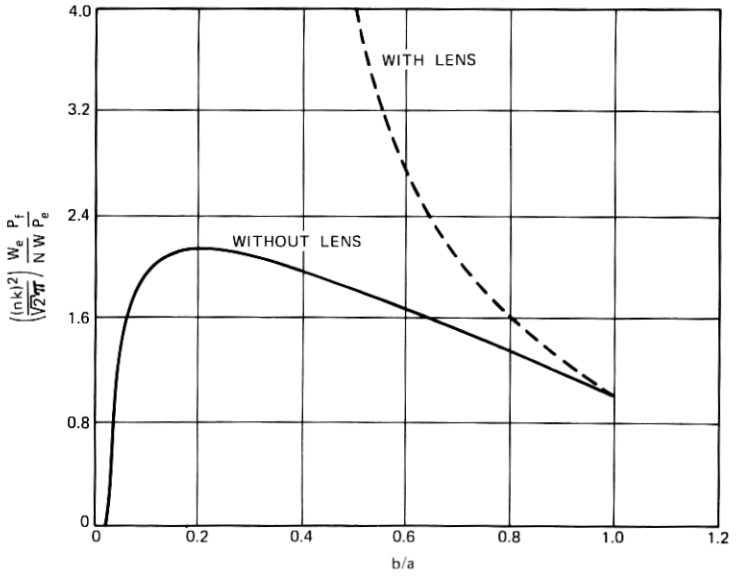

Fig. 15—Normalized ratio of total power injected into the fiber, P_f, relative to the electrical drive power P of the diode as a function of the (normalized) source radius. The solid curve applies for an LED in direct contact with the fiber; the dotted curve describes operation with a matching lens.

jected power is the loss of total source area. However, by bringing the source in direct contact with the fiber, a large amount of power is lost, because the fiber can trap only rays emitted at certain small maximum angles whose values depend on the point at which the ray is entering the fiber core. If we remove the source from the end of the fiber and focus its light onto the fiber end with a matching lens, we may increase the source image to make it coincide with the fiber core radius, but at the same time we inject all rays at a smaller angle. The loss in source brightness, caused by the magnification of its image, is thus compensated for by the fact that many of the rays, those that left the diode at angles too large to be trapped when the source was in direct contact with the fiber, are now transformed to smaller angles so that a wider cone of light leaving the source is able to be accepted by the fiber.

To investigate the beneficial effect of a matching lens, we use the transformation laws of Laguerre-gaussian beams that have been formulated by Kogelnik.[11] We assume that the source is imaged by a lens onto the end of the fiber as shown in Fig. 16. The transformation laws of gaussian beams[3,11] yield the result (in agreement with geometrical optics) that the beamwidth parameter w_0 of the fiber mode is transformed to the width w given by

$$w = \frac{b}{b'} w_0. \tag{40}$$

The source radius b has been transformed by the lens to the radius of its image b'; w_0 is given by (19). We can evaluate the effect of the matching lens by writing (30) (with $d = 0$) in the form

$$P\langle |c_{\nu,p}|^2 \rangle = \frac{2\pi^2 B}{(nk)^2} \frac{p!}{(p+\nu)!} \int_0^{2b^2/w^2} u^\nu e^{-u} [L_p^{(\nu)}(u)]^2 du. \tag{41}$$

Equation (41) expresses the amount of power in one mode. The total

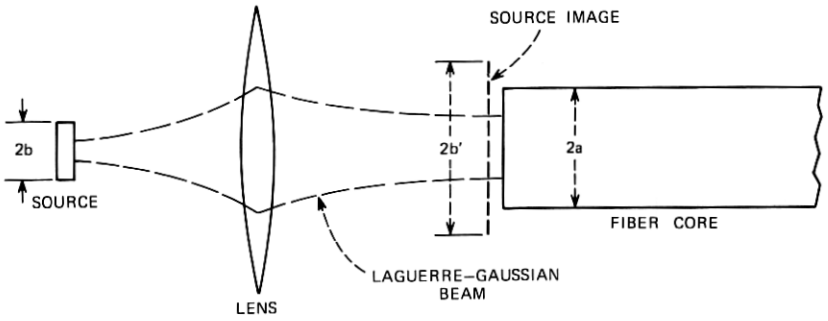

Fig. 16—Launching geometry with a matching lens.

power injected into the fiber is obtained by summing over all the guided modes. The beamwidth parameter w of the transformed Laguerre-gaussian beam enters this expression only in the upper limit of the integral. The critical term to consider is thus

$$u_1 = 2\frac{b^2}{w^2} = 2\frac{b'^2}{w_0^2}. \tag{42}$$

Equation (41) is of exactly the same form as the expression (30) for $d = 0$ in the absence of the lens. Only the beamwidth w at the position of the source is important. Choosing the lens in such a way that the image size b' of the source becomes equal to the fiber core radius ($b' = a$) results in $u_1 = 2a^2/w_0$. This means that the launching efficiency through the matching lens is identical to the launching efficiency for a source with $b = a$ in direct contact with the fiber, even though the size of the source in Fig. 16 is smaller than the fiber radius. In fact, we know from Fig. 10 that the excitation efficiency is not changed even if the source is made larger than the fiber core. The same is true for the image of the source projected onto the fiber end through the matching lens. Even if we project a source image that is larger than the fiber end, the launching efficiency is maintained if the source brightness (of the original, not the imaged source) is held constant. This seemingly contradictory result is caused by the fact that more and more rays arrive at the fiber end at smaller angles with respect to the fiber axis, making up the loss in image brightness that is caused by the larger lens magnification. This constancy of the launching efficiency, which is achievable with a matching lens, breaks down only when the lens must be so far removed from the fiber that some of the light power, which would radiate from the fiber (if we reverse the direction of all the light beams), begins to miss the lens boundary.

Thus, we have reached the conclusion that a matching lens can improve the launching efficiency of a small source to such a degree that we can obtain as much power as would be available from a large source in contact with the fiber. The total coupling efficiency with respect to the electrical power used by the diode may be considerably improved with the help of a matching lens. Instead of (39), a matching lens allows us to achieve the power ratio

$$\frac{P_f}{P_e} = \frac{2\pi^2 NW}{(nk)^2 W_e}\frac{1}{(b/a)^2}. \tag{43}$$

Equation (43) is plotted as the dotted curve in Fig. 15. This expression does not contain the effect of the finite lens aperture that must be considered for very large magnification. Equation (43) indicates that a matching lens would allow us to achieve higher launching efficiencies

than may be achieved by placing the LED directly in contact with the fiber.

Instead of a lens, a tapered dielectric waveguide of high refractive index difference between core and cladding material may be used to match a small LED to a larger fiber core. However, any optical matching device complicates the basically simple configuration of an LED in direct contact with the fiber. For many applications, it may be more advantageous to suffer the additional coupling loss that results by forgoing the procedure of matching the source to the fiber size. Incidentally, a matching lens does not increase the amount of power that may be injected from a large source.

VII. CONCLUSIONS

We have studied the excitation of parabolic-index fibers with incoherent light sources and found that a source, whose area covers the cross section of the fiber core, injects equal power into all the modes. As the source is moved away from the fiber end, it injects relatively less power (without a lens) into higher-order (as compared to low-order) modes. However, the injection mechanism is quite tolerant of source-fiber separation. At a distance of five fiber-core diameters (assuming $b/a = 1$ and $\Delta = 0.01$), the total amount of power injected into the fiber core decreases only to one-half the amount that can be achieved if the source is placed directly in contact with the diode. If the source is transversely displaced, the amount of power launched into the fiber drops to about one-half of its maximum value for a source displacement equal to the fiber radius, if the source is in contact with the fiber.

Without a matching lens, the amount of power launched into the fiber decreases with decreasing source radius (if $b/a < 1$). However, since the brightness achievable from an LED increases with decreasing radius, an optimum radius for maximum light-power injection into the fiber is obtained at a source-to-core radius ratio of $b/a = 0.8$. Relative to the electrical power requirements of the diode, the launching efficiency is optimized at $b/a = 0.2$. A compromise between these two optima may be to choose the ratio $b/a = 0.5$. These numbers are based on a special high-brightness LED developed by Burrus.[10]

Use of a matching lens allows us to inject the same amount of power from a small LED that would be available from a large source of equal brightness in direct contact with the fiber. However, because the achievable brightness increases with the decreasing radius of an LED more power can be obtained from a small LED whose light is focused into the fiber with a lens. Use of a matching lens also increases the overall efficiency of operation as shown by the dotted line in Fig. 15.

However, matching lenses or tapers complicate the basically simple launching geometry of an LED in direct contact with the fiber.

VIII. ACKNOWLEDGMENT

We profited from several valuable discussions with E. A. J. Marcatili and C. A. Burrus. Mr. Marcatili suggested the possibility of optimizing the source radius without a matching lens.

APPENDIX

We sketch the derivation of eq. (8). The plane-wave modes of free space can be expressed as[12]

$$\mathbf{E}_{\kappa,\sigma} = \frac{(2\omega\mu_0 P)^{\frac{1}{2}}}{2\pi\sqrt{\beta}} \mathbf{e} e^{-i(\kappa x+\sigma y+\beta z)} \tag{44}$$

with

$$\beta^2 = n^2k^2 - \kappa^2 - \sigma^2. \tag{45}$$

From (7) we obtain, by substitution of (44),

$$P\langle|c|^2\rangle = \frac{\omega\mu_0}{32\pi^2\beta} StA_s. \tag{46}$$

The total power radiated by the source is obtained from the formula:[13]

$$P_r = 2\int\int_{-\infty}^{\infty} P\langle|c|^2\rangle d\kappa d\sigma. \tag{47}$$

The factor 2 accounts for the two possible polarizations. We may express the differentials of the integral in terms of the element of solid angle $d\Omega$ into which the radiation is directed,[14]

$$d\kappa d\sigma = nk\beta d\Omega. \tag{48}$$

Thus, the fractional amount of power radiated into the element of solid angle is

$$\Delta P_r = 2P\langle|c|^2\rangle nk\beta d\Omega. \tag{49}$$

Substitution of (46) into (49) results in (8).

REFERENCES

1. K. H. Yang and J. D. Kingsley, "Calculation of Coupling Losses Between Light Emitting Diodes and Low Loss Optical Fibers," Applied Optics, *14*, No. 2 (February 1975), pp. 288–293.
2. P. Di Vita and R. Vannucci, "Geometrical Theory of Coupling Errors in Dielectric Optical Waveguides," Optics Communication, *14*, No. 1 (May 1975), pp. 139–144.
3. D. Marcuse, *Light Transmission Optics*, New York: Van Nostrand Reinhold, 1972.
4. D. Marcuse, *Theory of Dielectric Optical Waveguides*, New York: Academic Press, 1974.

5. R. E. Collin, *Foundations for Microwave Engineering*, New York: McGraw-Hill, 1966, eq. (4.84a), p. 185.
6. G. Goubau and F. Schwering, "On the Guided Propagation of Electromagnetic Beam Waves," IRE Trans. on Antennas and Propagation, *AP-9*, No. 3 (May 1961), pp. 248–256.
7. H. Kogelnik and T. Li, "Laser Beams and Resonators," Applied Optics, *5*, No. 10 (October 1966), pp. 1550–1567.
8. I. S. Gradshteyn and I. M. Ryzhik, *Tables of Integrals, Series and Products*, 4th edition, New York: Academic Press, 1965, p. 1037.
9. C. N. Kurtz and W. Streifer, "Guided Waves in Inhomogeneous Focusing Media, Part I: Formulation, Solution for Quadratic Inhomogeneity," IEEE Trans. Microwave Theory and Techniques, *MTT-17*, No. 1 (January 1969), pp. 11–15.
10. C. A. Burrus, "Radiance of Small-Area High-Current-Density Electroluminescent Diodes," Proc. IEEE, *60*, No. 2 (February 1972), pp. 231–232.
11. H. Kogelnik, "Imaging of Optical Modes—Resonators with Internal Lenses," B.S.T.J., *44*, No. 3 (March 1965), pp. 455–494.
12. Ref. 3, eq. (4.7-1), p. 168.
13. Ref. 3, eq. (4.7-13), p. 169.
14. Ref. 3, eq. (4.7-15), p. 170.